ARTICLES SCIENCE CHINA Materials

mater.scichina.com link.springer.com

Published online 17 January 2019 | https://doi.org/10.1007/s40843-018-9386-8

Sci China Mater 2019, 62(7): 936–946

Compact self-standing layered film assembled by V_2O_5·*n*H_2O/CNTs 2D/1D composites for high volumetric capacitance flexible supercapacitors

Kai Guo[1,4], Yiju Li[2], Chong Li[3], Neng Yu[1*] and Huiqiao Li[4*]

ABSTRACT **Flexible supercapacitors (SCs) are attractive energy storage devices for wearable electronics, but their applications are hindered by their low volumetric energy densities. Two dimensional (2D) non-carbon nanomaterials are the most promising pseudocapacitive materials for high volumetric capacitance electrodes. However, they are poorly conductive and prone to self-stacking, which results in unsatisfactory electrochemical performance. In this work, large-scale V_2O_5·*n*H_2O ultrathin nanosheets are synthesized by a facile and scalable method and transformed into layered and compact composite films with one-dimensional carbon nanotubes (CNTs). The self-standing films show an optimized volumetric capacitance of 521.0 F cm^{-3} with only 10 wt% of CNTs, which is attributed to dramatically enhanced electrical conductivity beyond the electrical percolation threshold, high dispersion of pseudocapacitive V_2O_5·*n*H_2O nanosheets, and high mass density of the films. All-solid-state flexible SCs made of V_2O_5·*n*H_2O/CNTs films show a maximum energy density of 17.4 W h L^{-1}.**

Keywords: flexible supercapacitors, volumetric capacitance, two-dimensional nanosheets, vanadium pentoxide, layered structure

INTRODUCTION

The rapid development of wearable electronics urgently triggers the demands for flexible and compact energy storage devices [1–7]. Flexible supercapacitors (SCs) are promising power sources due to superior advantages of high power density, fast charging rate, long life, excellent flexibility and miniature size [8–15]. However, their low energy density hinders their broad applications. Most of the current work focuses on increasing their gravimetric energy density rather than their volumetric energy density [16–20]. In fact, the volumetric energy density is a more reasonable measure gauge and a more important parameter than the gravimetric energy density for practical applications of flexible SCs [21–26]. Therefore, it is very urgent to enhance the volumetric energy density of flexible SCs.

Flexible electrodes with high volumetric capacitance is the key to achieve high volumetric energy density flexible SCs. Since the volumetric capacitance is the product of the density and the gravimetric capacitance, a flexible compact film with a high gravimetric capacitance makes a high volumetric capacitance electrode for flexible SCs. Recently, emerging two dimensional (2D) nanomaterials are promisingly high volumetric capacitance electrodes due to the ultra-high surface volume atom ratio, large specific surface area, high electrochemical activities and, especially, excellent feasibility in assembling compact flexible films by layer-by-layer stacking compared to one-dimensional nanomaterial [24,27–30]. Graphene is currently the most attractive 2D material in constructing high volumetric electrodes [22,31–33]. Unfortunately, the electric double-layer storage mechanism of graphene greatly limits its capacitance. In contrast, 2D pseudocapacitive materials with rather high gravimetric capacitance and density show tremendous potential in fabricating high volumetric capacitance film electrodes. However, most of the pseudocapacitive materials are non-

[1] Jiangxi Province Key Laboratory of Polymer Micro/Nano Manufacturing and Devices, School of Chemistry, Biology and Materials Science, East China University of Technology, Nanchang 330013, China

[2] Department of Materials Science and Engineering, College of Engineering, Peking University, Beijing 100871, China

[3] Wuhan National Laboratory for Optoelectronics, School of Optics and Electronic Information, Huazhong University of Science and Technology, Wuhan 430074, China

[4] State Key Laboratory of Material Processing and Die & Mould Technology, School of Materials Science and Engineering, Huazhong University of Science and Technology, Wuhan 430074, China

* Corresponding authors (emails: neng063126@ecit.cn (Yu N); hqli@hust.edu.cn (Li H))

conductive or semi-conductive and tend to closely stacked due to strong in-plane interaction just like graphene [34–36]. In addition, scalable synthesis of high-quality 2D pseudocapacitive nanomaterials is still costly, due to long-time exfoliation of bulk materials and low-productivity centrifugation [28,37–41]. Thus, it is a big challenge to build a 2D pseudocapacitive material-based film with high conductivity and density for high volumetric density flexible supercapacitors.

Among various pseudocapacitive materials, V_2O_5 attracts much attention because of high electrochemical activity, high capacity, multiple valence states (from +2 to +5), controllable morphology, and a substantial deposit [42–45]. Layer-type hydrated vanadium pentoxides ($V_2O_5{\cdot}nH_2O$) has a variable interlayer spacing ranging from 8.8 to 13.8 Å. This special layer structure is feasible for mono- or multi-valence ions intercalation, which enables the high potential for the synthesis of high surface 2D $V_2O_5{\cdot}nH_2O$ nanosheets. Besides, the vanadium oxide species are known as large capacity electrode candidates due to their multi-valence states [46–49], which might contribute to a large pseudo-capacitance in a capacitor.

Herein, large-scale ultrathin $V_2O_5{\cdot}nH_2O$ nanosheets have been facilely synthesized through a scalable hydrothermal reaction. Then, layered compact self-standing $V_2O_5{\cdot}nH_2O$/carbon nanotubes (CNTs) 2D/1D composite films with different mass ratios can be easily obtained by the vacuum self-assembled filtration. The conductivity, density, layer gaps, and electrochemical performance of the composite films can be well controlled by the mass ratio of CNTs. When the mass ratio of CNTs reaches 10 wt%, the volumetric capacitance of the composite film is optimized to 521.0 F cm^{-3}, which is comparable or even superior to many recent results. The high volumetric capacitance can be attributed to a high mass loading of $V_2O_5{\cdot}nH_2O$, dramatically enhanced electrical conductivity or electrical percolation effect, high dispersion of pseudocapacitive $V_2O_5{\cdot}nH_2O$ nanosheets, and a high density. The composite films are also highly flexible and assembled into flexible SCs, which has a maximum volumetric energy of 17.4 W h L^{-1}.

EXPERIMENTAL SECTION

Synthesis of $V_2O_5{\cdot}nH_2O$ aerogel

V_2O_5 (0.36 g) powder was dispersed in 30 mL deionized water and then 16.5 mL H_2O_2 solution was added in. After stirring for 2 h, the solution became transparent and orange and then was transferred to a 100-mL autoclave for hydrothermal reaction at 200°C for 16 h. The reddish-brown hydrothermal product, $V_2O_5{\cdot}nH_2O$ hydrogel, went through freeze-drying for 24 h to make a reddish-brown aerogel.

Fabrication of $V_2O_5{\cdot}nH_2O$/CNTs composite films

$V_2O_5{\cdot}nH_2O$ aerogel and CNTs aqueous solution were dispersed in 20 mL deionized water with stirring and vacuum filtration with 0.22 μm (pore size) cellulose membranes. The cellulose membranes were dried at 60°C for 10 min, and then the composite films were carefully peeled off from the filtration membranes. The total mass of $V_2O_5{\cdot}nH_2O$ and CNTs was 15 mg and their mass ratios were 0:100, 5:95, 10:90, 15:85, and 100:0. The corresponding films were named CNT, VC-5%, VC-10%, VC-15%, and $V_2O_5{\cdot}nH_2O$ film, respectively. The CNT and $V_2O_5{\cdot}nH_2O$ films were control samples.

Assembly of flexible SCs

Polyethylene terephthalate (PET) films (10 μm thickness) were deposited with Cr/Au (10/50 nm, through electron beam sputtering) and were used as current collectors. The film samples were cut into disks of 10 mm in diameter and were attached to PET/Au films with the assistance of ethanol. Then, a piece of filter paper soaked with polyvinyl alcohol (PVA)/$LiClO_4$ gel electrolyte was tightly sandwiched by two PET films and then dried at 60°C to remove excess water.

Characterizations

The V_2O_5 aerogel and $V_2O_5{\cdot}nH_2O$/CNTs films were characterized with X-ray diffractometer (XRD, X'Pert PRO, PANAlytical B.V.), scanning electron microscopy (SEM, Quanta 650, FEI), X-ray photoelectron spectrum (XPS, AXIS-ULTRA DLD-600W, Kratos), and atomic force microscopy (AFM, Dimension XR, Bruke), respectively. The conductivity of film samples was characterized by a four-probe conductivity meter (Loresta-GX-MCP-T700, Mitsubishi Chemical). Cyclic voltammetry (CV), galvanostatic charging/discharging (GCD) and electrochemical impedance spectroscopy (EIS) of the film electrodes and SC devices were investigated on an electrochemical station (CHI 660E, USA). The electrochemical performance of film electrodes was tested with a three-electrode system in a $LiClO_4$ (1 mol L^{-1}) aqueous solution electrolyte with saturated calomel reference electrode (SCE) and Pt counter electrode (1 cm×1 cm). The working electrodes were prepared by cutting the film samples into 10 mm in diameter of film disks and then pressing the disks on the nickel foam with 2 MPa pressure. The specific capacitance of film electrodes and

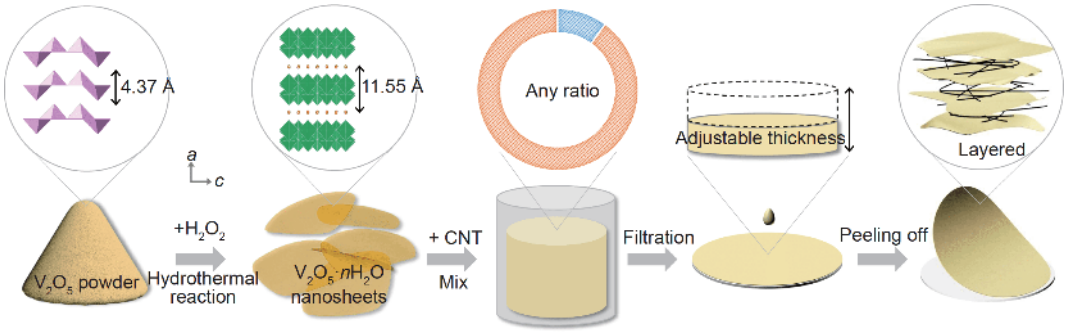

Figure 1 Schematic fabrication process of V_2O_5·nH_2O/CNTs composite films.

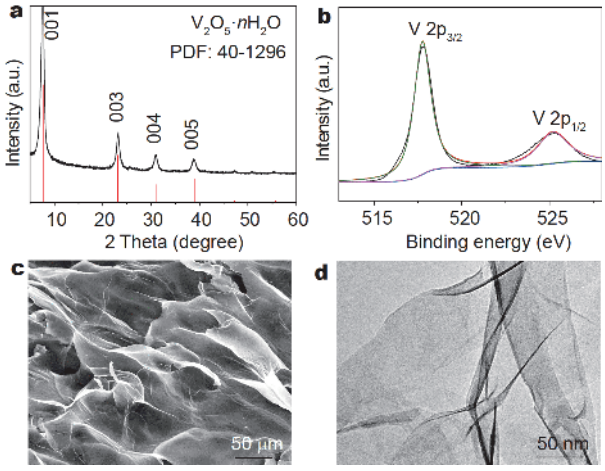

Figure 2 Characterization of V_2O_5·nH_2O aerogel: (a) XRD, (b) V 2p XPS spectrum, (c) SEM image and (d) TEM image.

SC devices were calculated based on the mass and volume of the round disk film samples.

RESULTS AND DISCUSSION

The fabrication process of V_2O_5·nH_2O/CNTs composite films is shown in Fig. 1. Firstly, yellow bulk V_2O_5 powder is transformed into reddish-brown layered hydrated V_2O_5 nanosheets facilely through a scalable hydrothermal reaction. Then freeze dried layered hydrated V_2O_5 nanosheets aerogel is mixed with CNT dispersion and vacuum-filtered to obtain flexible layer-structured films composed of 1D conductive CNTs and 2D pseudocapacitive nanosheets. This filtration method can freely adjust the composition and thickness of the composite films.

The XRD pattern of the V_2O_5 aerogel in Fig. 2a displays four peaks assigned to the hydrated layered V_2O_5·nH_2O phase (JCPDS No. 40-1296). The corresponding interplanar gap is 11.5 Å for the (001) plane, in consistence with n~1.6 calculated by using the diameter of water molecule (2.7 Å) [50]. The two peaks at 517.8 and 525.2 eV in V 2p XPS spectrum (Fig. 2b) are attributed to the binding energy of V $2p_{3/2}$ and V $2p_{1/2}$ orbitals, respectively, revealing that the valence state of V element is +5 [51]. The V_2O_5 aerogel is nanosheet-shaped with a lateral size of hundreds of micrometers (Fig. 2c). The TEM image in Fig. 2d confirms the morphology of V_2O_5·nH_2O aerogel and the thickness of V_2O_5·nH_2O nanosheet is ~3.6 nm, as shown in the AFM image (Fig. S1). The 2D nanosheets have abundant electrochemically reactive sites and a large contact area with the electrolyte, which can greatly improve the electrochemical performance.

CNTs are introduced to enhance the conductivity and to suppress the self-stacking of V_2O_5·nH_2O nanosheets simultaneously through intercalating CNTs in the interlayer of V_2O_5·nH_2O nanosheets. Typically, the resistance of a non-conductive phase and a conductive phase composite system decreases abruptly when the content of the conductive phase reaches a critical point. The phenomenon is called electrical percolation effect and the critical point of conductivity is called electrical percolation threshold [52]. The electrical percolation effect has an intensive impact on the specific capacitance of supercapacitor composite electrodes by affecting the resistance of composite materials [53,54]. In this work, the mass ratio of CNTs not only directly determines the conductivity but also controls the content of pseudocapacitive materials and the mass density of the composite films. By limiting the mass ratio of CNTs to 5–15 wt%, the composite films are compact and have a high density. The microstructure of the composite films is very different from that of the control samples. The composite films (Fig. 3c) have a denser surface than the porous CNT films (Fig. 3a) by filling the voids among CNTs with V_2O_5·nH_2O nanosheets, while the V_2O_5·nH_2O film composed of highly self-stacked nanosheets seems rather

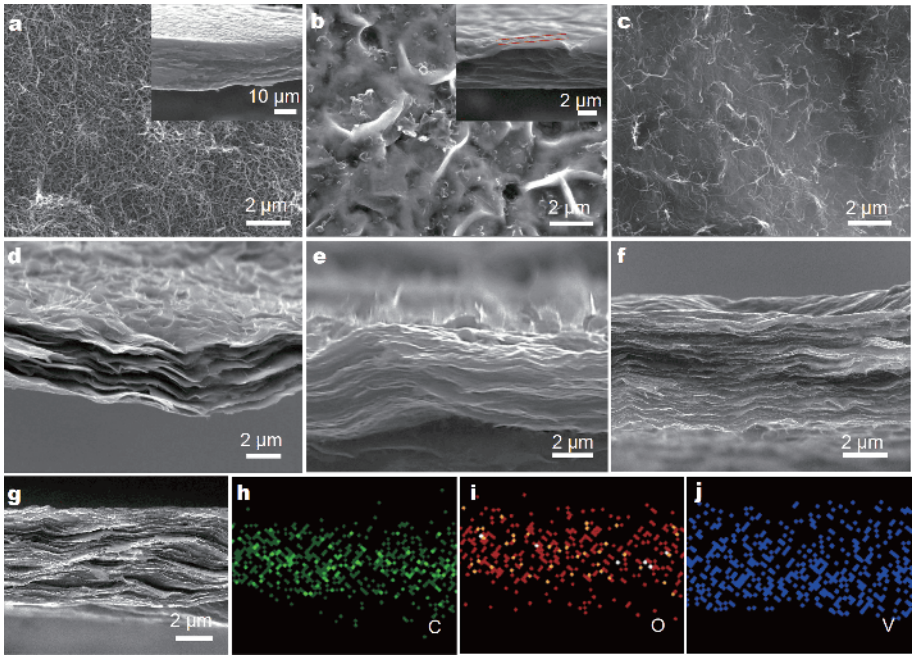

Figure 3 Top-view SEM images of (a) CNT, (b) $V_2O_5{\cdot}nH_2O$, and (c) VC-5% films. Inset in (a) and (b): the cross-section SEM image of the CNT and $V_2O_5{\cdot}nH_2O$ film, respectively. The cross-section SEM image of the (d) VC-5%, (e) VC-10%, and (f) VC-15% films. (g) Cross-section SEM image and the elemental mapping image of (h) C, (i) O, and (j) V elements in the composite film.

dense (Fig. 3b). In the cross-section view, the CNT film is monolithic and porous (inset in Fig. 3a and Fig. S2) and the $V_2O_5{\cdot}nH_2O$ nanosheets are highly stacked without voids or gaps (Fig. 3b). In contrast, all the composite films self-assemble into a layered structure in the axial direction, and both the thickness of the layers and the interlayer gaps of the composite films become smaller. In the meanwhile, the thickness of the film increases with mass ratio of CNTs (Fig. 3d–3f). The changes of the microstructure can be attributed to the well dispersion of the $V_2O_5{\cdot}nH_2O$ nanosheets with a high CNTs mass ratio, which is illustrated in the following content. Thick layers in the VC-5% are difficult for electrolyte infiltration, while thinner layers in VC-10% and VC-15% can increase electrolyte infiltration and shorten ion diffusion paths. To identify the dispersible uniformity of CNTs in the composite film, the elemental mapping was conducted on the specific position in Fig. 3g. The corresponding elemental distribution of C, O, and V elements is all uniform in the axial direction (Fig. 3h–3j), respectively. It indicates CNTs are uniformly dispersed between the $V_2O_5{\cdot}nH_2O$ nanosheets, which facilitates fast electron transportation in the whole film.

Besides the thickness, the conductivity and density of the films are also feasibly controlled by the mass ratio of CNTs. The square resistance decreases with a high CNT mass ratio, and the descent rate of the device with more than 10 wt% of CNTs becomes much faster (Fig. 4a). The square resistance of the pure $V_2O_5{\cdot}nH_2O$ film is $1.255\times10^6\ \Omega\ sq^{-1}$ and decreases by ~10,000 times to $128\ \Omega\ sq^{-1}$ in the VC-10% film, which is about 10 folds of square resistance of the CNT film. On the other side, the density of as-prepared films decreases while their thickness increases nonlinearly with a large mass ratio of CNTs, and the change rate is fast for both the density and thickness below 10 wt% of CNTs (Fig. 4b). A model (Fig. 4c) is proposed to explain the results. During the vacuum filtration, the conductive CNTs are dispersed into interlayers of $V_2O_5{\cdot}nH_2O$ nanosheets and attached to their surface, resulting in a layered structure. The CNTs on the surface can form a network in the planar direction of the composite film. In the meantime, a small content of CNTs cross the $V_2O_5{\cdot}nH_2O$ nanosheets and form electric conducting paths in the axial direction of the composite film. But they are not abundant to form a three-dimensional conducting network with only a small amount (5 wt% in this work). With 10 wt% of or more CNTs, a conducting network can be formed and the square resistance changes rapidly, as shown in the scheme in Fig. 4a. It suggests there is a threshold for the conductivity of the composite films, or the electric percolation effect is triggered around 10 wt% of CNTs.

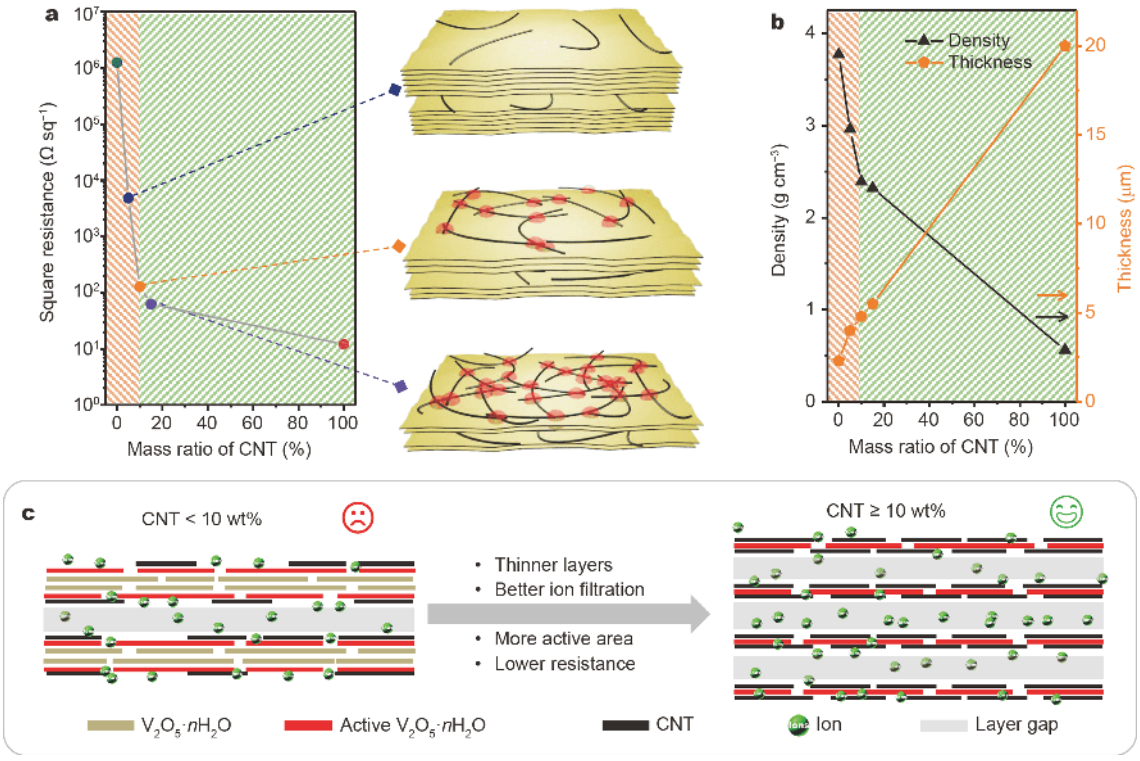

Figure 4 The effects of CNTs mass ratio on (a) the square resistance, (b) the density and thickness of different film samples. Schematic cross-section microstructure, ion diffusion, and electron transfer in composite films with (c) a small (5 wt%) and large amount (≥10 wt%) of CNTs. Schemes in (a): the microstructure of layered composite films with different ratio of CNTs (black lines) and $V_2O_5{\cdot}nH_2O$ nanosheets (yellow planes), in which the contact points of crossed CNTs are marked with red semi-spheres.

More CNTs in the composite films can further suppress the self-stacking of $V_2O_5{\cdot}nH_2O$ nanosheets, and therefore the thickness of the layers becomes smaller (Fig. 4c). Thinner layers render several advantages, including better ion infiltration into the $V_2O_5{\cdot}nH_2O$ nanosheets, more active $V_2O_5{\cdot}nH_2O$ nanosheets because of the larger exposed surface area, and lower resistance across the thinner stacking $V_2O_5{\cdot}nH_2O$ nanosheets.

The electrochemical performance of the films was characterized (Fig. 5). The CV curves of different films were conducted at 10 mV s^{-1} between −0.2–0.8 V (Fig. 5a). The VC-5% film displays a distorted rectangular CV curve, while the VC-10% and VC-15% films demonstrate quasi-rectangular CV curves with several redox peaks. The CNTs film shows a much smaller CV area than the composite films, while the CV curve of the $V_2O_5{\cdot}nH_2O$ film covers a negligible area, suggesting the two control samples are poorly capacitive. The gravimetric and volumetric capacitance of different films at 0.5–20 A g^{-1} is displayed in Fig. 5b and 5c, respectively. The CNTs film shows much smaller gravimetric and volumetric capacitance than the composite films because of the small specific surface area and electric double-layer storage mechanism. The electrochemical redox reaction of the pure $V_2O_5{\cdot}nH_2O$ film is seriously suppressed and the $V_2O_5{\cdot}nH_2O$ film nearly shows no capacitance, which can be attributed to its very low conductivity and poor ion diffusion induced by the highly self-stacking of $V_2O_5{\cdot}nH_2O$ nanosheets. It suggests the synergistic effect between the 1D CNTs and 2D $V_2O_5{\cdot}nH_2O$ nanosheets. Among the composite films, VC-10% film has the largest specific capacitance of 207.7 F g^{-1} or 521.0 F cm^{-3} at 0.5 A g^{-1}, revealing that the optimized ratio of CNTs in the composite film is 10 wt%. The capacitance retention of VC-5%, VC-10%, and VC-15% is 3.9%, 41.8%, and 49.5%, respectively, when the current density increases from 0.5 to 20 A g^{-1}, suggesting good rate performance of VC-10% and VC-15% films. It is worth noting that the rate performance of the three composite films upturns abruptly when the mass ratio of CNTs increases from 5 to 10 wt%. Therefore, the VC-10% shows the largest gravimetric and volumetric capacitance and moderate rate performance among the composite films.

There are three key factors determining the electro-

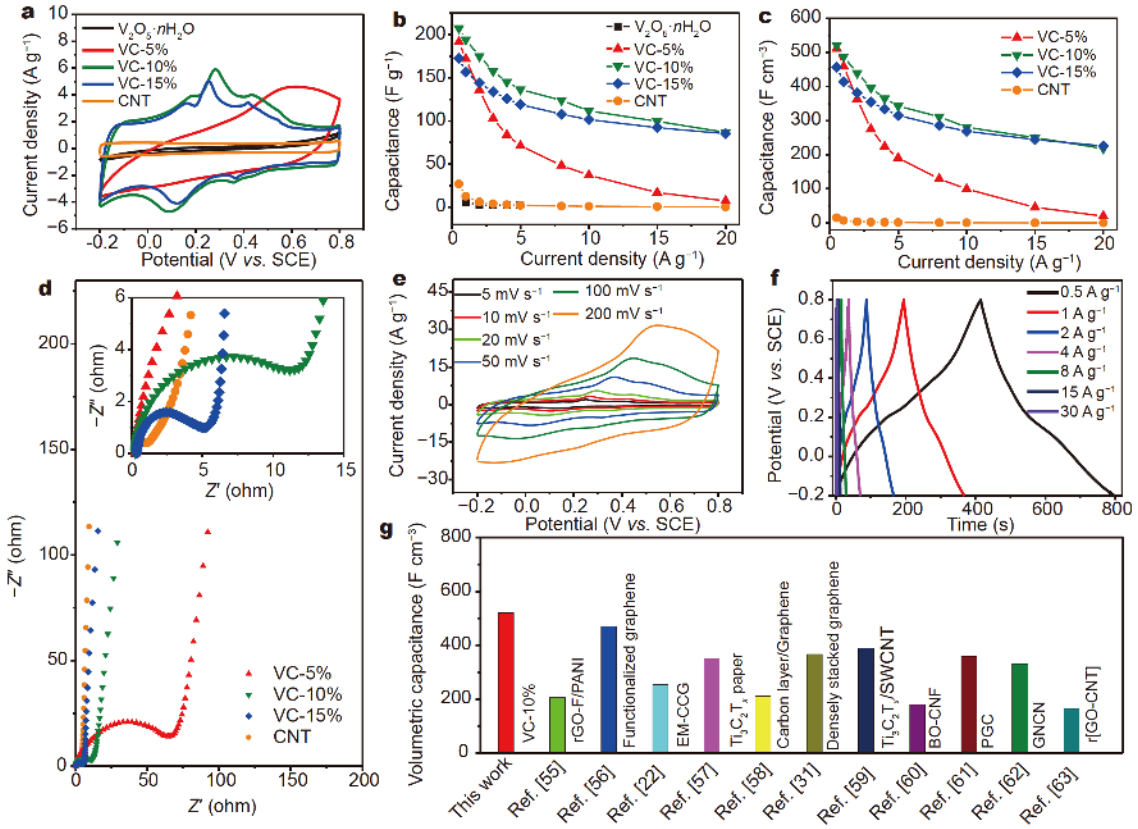

Figure 5 Electrochemical performances of different film samples. (a) CV curves, (b) gravimetric capacitance, (c) volumetric capacitance, and (d) EIS plots of different film samples. (e) CV and (f) GCD curves of the VC-10% film electrode. (g) The volumetric capacitance of different flexible film electrodes.

chemical performance of the CNT, $V_2O_5{\cdot}nH_2O$ and composite film electrodes: the conductivity, ion diffusion efficiency and pseudocapacitance. The CNT film shows good rate performance because of high conductivity and porosity but poor specific capacitance resulting from the electric double layer storage mechanism. The $V_2O_5{\cdot}nH_2O$ film can hardly display capacitance because of very low conductivity and serious self-stacking. Although the VC-5% has a high $V_2O_5{\cdot}nH_2O$ mass ratio, its specific capacitance is not high at a large discharging current density, which can be attributed to the high resistance and high stacking of $V_2O_5{\cdot}nH_2O$ nanosheets. The obviously enhanced electrochemical performance of VC-10% is attributed to the abrupt decrease of resistance in the device with 10 wt% CNTs derived from the electric percolation effect and improved dispersion of $V_2O_5{\cdot}nH_2O$ nanosheets, which can be proved by the EIS plots in Fig. 5d. A much larger diameter of the semi-circle in the middle-frequency range and smaller tilt angle of the straight line in the low frequency range (as shown in the inset) of the spectrum for VC-5% reveals larger electron transport and ion diffusion resistance than those of VC-10% [55]. More CNTs in the VC-15% leads to smaller gravimetric and volumetric specific capacitance because of lower pseudocapacitance and density, compared with VC-10%.

Detailed electrochemical performance of VC-10% is presented in Fig. 5e and 5f. The shapes of the CV curves of VC-10% at 5–200 mV s^{-1} are distorted rectangles with several peaks (Fig. 5e). The GCD curves in Fig. 5f are very close to symmetric triangles with several slopes corresponding to the peaks in the CV curves. The VC-10% shows a gravimetric capacitance of 207.7 F g^{-1} and a very high density of 2.4 g cm^{-3}. Because of the very high density, the volumetric capacitance of VC-10% is comparable or even superior to recent results, such as reduced graphene oxide/polyaniline composite (rGO-F/PANI, 205.4 F cm^{-3}), [55] functionalized graphene (470 F cm^{-3}) [56], liquid electrolyte-mediated chemically converted graphene (EM-CCG, 255.5 F cm^{-3}) [22], $Ti_3C_2T_x$ paper (350 F cm^{-3}) [57], porous carbon layer/graphene (212 F cm^{-3}) [58], densely stacked graphene

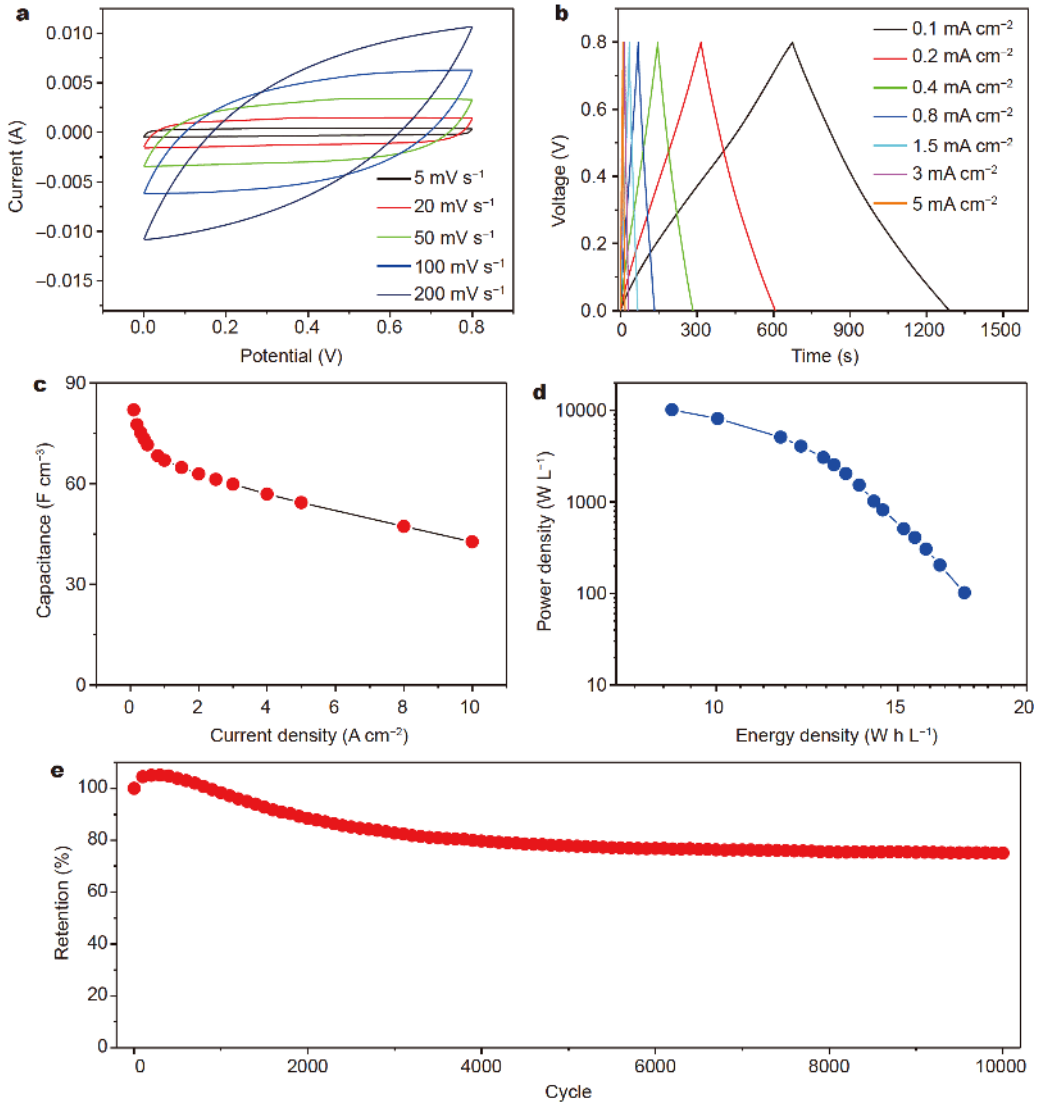

Figure 6 Electrochemical performance of symmetric SCs based on VC-10% film: (a) CV curves, (b) GCD curves, (c) volumetric capacitance, (d) gravimetric Ragone plot and (e) cycling performance.

(366 F cm^{-3}) [31], $Ti_3C_2T_x$/single-wall CNT film 390 F cm^{-3} [59], boron and oxygen co-doped carbon nanofiber (BO-CNF, 179.3 F cm^{-3}) [60], porous graphene-like carbon (PGC, 360 F cm^{-3}) [61], graphene nanomesh carbon nanotube hybrid film (GNCN, 331 F cm^{-3}) [62], and reduced graphene oxide/CNT composite film (165 F cm^{-3}) [63], as shown in Fig. 5g and Table S1.

Two VC-10% films were assembled into an all-solid-state flexible SC with PVA/$LiClO_4$ gel electrolyte. The CV curves of the SC at 0–0.8 V are close to rectangles at 5–100 mV s^{-1} or inclined rectangles even at 200 mV s^{-1} (Fig. 6a), indicating good rate performance of the device. The GCD curves are symmetric triangles, which is consistent with the CV curves. The rate performance calculated from the GCD curves is as shown in Fig. 6b. The specific capacitance of the device at the current density of 0.1 mA cm^{-2} is 34.3 F g^{-1} or 81.9 F cm^{-3}, and retains 52% of capacity when the current density increases to 10 mA cm^{-2} (Fig. 6c), suggesting excellent rate performance. The maximum energy density of the device is 7.3 kW h kg^{-1} (at 42.6 W kg^{-1}) or 17.4 W h L^{-1} (at 101.9 W L^{-1}), and the maximum power density of the device is 4,264.0 W kg^{-1} (at 3.8 W h kg^{-1}) or 10,191 W L^{-1} (9.1 W h L^{-1}), as displayed in Fig. 6d and Fig. S3. The cycling test of the device was carried out at the current

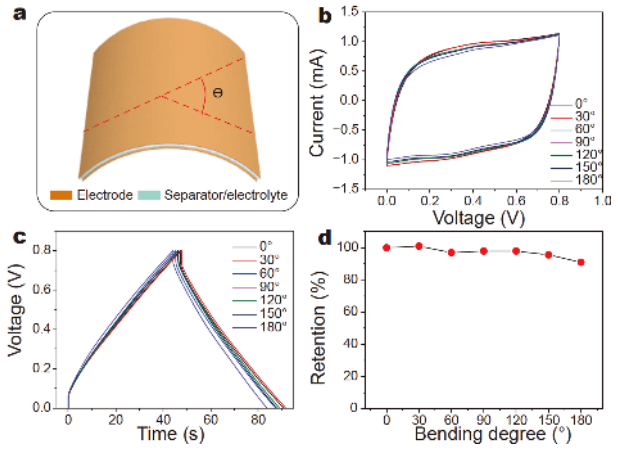

Figure 7 Flexibility characterization of flexible SCs. (a) Scheme of a bent flexible SC. (b) The CV curves, (c) GCD curves, and (d) capacitance retention of a flexible SC bent to different degrees.

density of 2 mA cm^{-2}. The device goes through an activation process and the capacitance increases to 105% of the initial value after the initial 300 cycles. Then the capacity of the device decays slowly and remains 75% of initial capacity after 10,000 cycles (Fig. 6e), suggesting good cycling performance.

Besides the electrochemical performance, the flexibility is another important issue of the flexible SCs. The symmetric SC was bent to different degrees to examine the flexibility (Fig. 7a and Fig. S4). The CV curves of the device being bent from 0° to 180° are almost coincident (Fig. 7b) with small differences in the GCD curves at different bending degrees (Fig. 7c). The capacitance loss at different bending states (Fig. 7d) calculated according to the GCD curves is less than 10%. The supercapacitor was then bent to 120° for 1,000 times. The capacitance retention decreases slowly to ~94% after 1,000 bending cycles (Fig. S5a), while the equivalent series impedance increases slowly from 3.6 to 9.0 Ω (Fig. S5b). The supercapacitor was also twisted to different degrees (Fig. S6), and more than 96% of capacitance is retained at even 90° of torsion (Fig. S7). Both the bending and torsion results indicate the supercapacitor has good flexibility and electrochemical stability under deformation, which is mainly attributed to good flexibility and mechanical stability of the VC-10% film.

CONCLUSIONS

In summary, compact self-standing layered flexible films composed of large-scale $V_2O_5{\cdot}nH_2O$ 2D nanosheets and 1D CNTs were successfully assembled through a facile and scalable vacuum filtration. The CNTs were dispersed into the interlayer of the nanosheets to form a conductive network and reduce their self-stacking. The special layered 2D/1D composite structure thus ensures good electric conductivity and ion diffusion, which improves the pseudocapacitance of 2D $V_2O_5{\cdot}nH_2O$. The thickness, density, conductivity, and the pseudocapacitance are controlled by the mass ratio of CNT. With 10 wt% of CNT, the volumetric capacitance of the composite film is optimized to 521.0 F cm^{-3} which can be attributed to the high pseudocapacitance from a large amount of $V_2O_5{\cdot}nH_2O$, dramatically enhanced electrical conductivity beyond the electrical percolation threshold, and a high density. The composite films are also highly flexible and can be assembled into flexible symmetric SCs with a maximum volumetric energy of 17.4 W h L^{-1} and stable electrochemical performance under different bending states. This work demonstrates an efficient solution for constructing high volumetric capacitance flexible electrodes by making the most of pseudocapacitance in 2D pseudo-capacitive materials.

Received 9 November 2018; accepted 17 December 2018; published online 17 January 2019

1 Wang X, Lu X, Liu B, *et al.* Flexible energy-storage devices: design consideration and recent progress. Adv Mater, 2014, 26: 4763–4782
2 Wang Y, Xia Y. Recent progress in supercapacitors: from materials design to system construction. Adv Mater, 2013, 25: 5336–5342
3 Xue Q, Sun J, Huang Y, *et al.* Recent progress on flexible and wearable supercapacitors. Small, 2017, 13: 1701827–1701837
4 Huang Y, Zhu M, Huang Y, *et al.* Multifunctional energy storage and conversion devices. Adv Mater, 2016, 28: 8344–8364
5 Yu N, Yin H, Zhang W, *et al.* High-performance fiber-shaped all-solid-state asymmetric supercapacitors based on ultrathin MnO_2 nanosheet/carbon fiber cathodes for wearable electronics. Adv Energy Mater, 2016, 6: 1501458
6 Guo K, Yu N, Hou Z, *et al.* Smart supercapacitors with deformable and healable functions. J Mater Chem A, 2017, 5: 16–30
7 Guo K, Wang X, Hu L, *et al.* Highly stretchable waterproof fiber asymmetric supercapacitors in an integrated structure. ACS Appl Mater Interfaces, 2018, 10: 19820–19827
8 El-Kady MF, Strong V, Dubin S, *et al.* Laser scribing of high-performance and flexible graphene-based electrochemical capacitors. Science, 2012, 335: 1326–1330
9 Lu X, Yu M, Wang G, *et al.* Flexible solid-state supercapacitors: design, fabrication and applications. Energy Environ Sci, 2014, 7: 2160–2181
10 Lv Z, Luo Y, Tang Y, *et al.* Editable supercapacitors with customizable stretchability based on mechanically strengthened ultralong MnO_2 nanowire composite. Adv Mater, 2018, 30: 1704531
11 Yu N, Guo K, Zhang W, *et al.* Flexible high-energy asymmetric supercapacitors based on MnO@C composite nanosheet electrodes. J Mater Chem A, 2017, 5: 804–813
12 Guo K, Wan Y, Yu N, *et al.* Hand-drawing patterned ultra-thin integrated electrodes for flexible microsupercapacitors. Energy

Storage Mater, 2018, 11: 144–151
13 Guo K, Ma Y, Li H, *et al.* Flexible wire-shaped supercapacitors in parallel double helix configuration with stable electrochemical properties under static/dynamic bending. Small, 2016, 12: 1024–1033
14 Sun H, Xie S, Li Y, *et al.* Large-area supercapacitor textiles with novel hierarchical conducting structures. Adv Mater, 2016, 28: 8431–8438
15 Zhang Y, Bai W, Cheng X, *et al.* Flexible and stretchable lithium-ion batteries and supercapacitors based on electrically conducting carbon nanotube fiber springs. Angew Chem Int Ed, 2014, 53: 14564–14568
16 Zhai T, Lu X, Wang H, *et al.* An electrochemical capacitor with applicable energy density of 7.4 Wh/kg at average power density of 3000 W/kg. Nano Lett, 2015, 15: 3189–3194
17 Xia X, Zhang Y, Chao D, *et al.* Tubular TiC fibre nanostructures as supercapacitor electrode materials with stable cycling life and wide-temperature performance. Energy Environ Sci, 2015, 8: 1559–1568
18 Zhu W, Li R, Xu P, *et al.* Vanadium trioxide@carbon nanosheet array-based ultrathin flexible symmetric hydrogel supercapacitors with 2 V voltage and high volumetric energy density. J Mater Chem A, 2017, 5: 22216–22223
19 Li Q, Lu C, Chen C, *et al.* Layered $NiCo_2O_4$/reduced graphene oxide composite as an advanced electrode for supercapacitor. Energy Storage Mater, 2017, 8: 59–67
20 Yang J, Xiong P, Zheng C, *et al.* Metal-organic frameworks: A new promising class of materials for a high performance supercapacitor electrode. J Mater Chem A, 2014, 2: 16640–16644
21 Wang Y, Yang X, Pandolfo AG, *et al.* High-rate and high-volumetric capacitance of compact graphene-polyaniline hydrogel electrodes. Adv Energy Mater, 2016, 6: 1600185–1600190
22 Yang X, Cheng C, Wang Y, *et al.* Liquid-mediated dense integration of graphene materials for compact capacitive energy storage. Science, 2013, 341: 534–537
23 Yan J, Ren CE, Maleski K, *et al.* Flexible MXene/graphene films for ultrafast supercapacitors with outstanding volumetric capacitance. Adv Funct Mater, 2017, 27: 1701264–1701273
24 Li H, Tao Y, Zheng X, *et al.* Ultra-thick graphene bulk supercapacitor electrodes for compact energy storage. Energy Environ Sci, 2016, 9: 3135–3142
25 Qin J, Zhou F, Xiao H, *et al.* Mesoporous polypyrrole-based graphene nanosheets anchoring redox polyoxometalate for all-solid-state micro-supercapacitors with enhanced volumetric capacitance. Sci China Mater, 2017, 61: 233–242
26 Wu S, Zhu Y. Highly densified carbon electrode materials towards practical supercapacitor devices. Sci China Mater, 2016, 60: 25–38
27 Ghidiu M, Lukatskaya MR, Zhao MQ, *et al.* Conductive two-dimensional titanium carbide 'clay' with high volumetric capacitance. Nature, 2014, 3: 78–81
28 Acerce M, Voiry D, Chhowalla M. Metallic 1T phase MoS_2 nanosheets as supercapacitor electrode materials. Nat Nanotechnol, 2015, 10: 313–318
29 Liu Y, Wang W, Huang H, *et al.* The highly enhanced performance of lamellar WS_2 nanosheet electrodes upon intercalation of single-walled carbon nanotubes for supercapacitors and lithium ions batteries. Chem Commun, 2014, 50: 4485–4488
30 Liu Y, Wang W, Wang Y, *et al.* Homogeneously assembling like-charged WS_2 and GO nanosheets lamellar composite films by filtration for highly efficient lithium ion batteries. Nano Energy, 2014, 7: 25–32
31 Sheng L, Jiang L, Wei T, *et al.* High volumetric energy density asymmetric supercapacitors based on well-balanced graphene and graphene-MnO_2 electrodes with densely stacked architectures. Small, 2016, 12: 5217–5227
32 Li H, Tao Y, Zheng X, *et al.* Compressed porous graphene particles for use as supercapacitor electrodes with excellent volumetric performance. Nanoscale, 2015, 7: 18459–18463
33 Li N, Lv T, Yao Y, *et al.* Compact graphene/MoS_2 composite films for highly flexible and stretchable all-solid-state supercapacitors. J Mater Chem A, 2017, 5: 3267–3273
34 Gu L, Wang Y, Lu R, *et al.* Anodic electrodeposition of a porous nickel oxide-hydroxide film on passivated nickel foam for supercapacitors. J Mater Chem A, 2014, 2: 7161–7164
35 Cheng X, Gui X, Lin Z, *et al.* Three-dimensional α-Fe_2O_3/carbon nanotube sponges as flexible supercapacitor electrodes. J Mater Chem A, 2015, 3: 20927–20934
36 Wu Y, Gao G, Wu G. Self-assembled three-dimensional hierarchical porous V_2O_5/graphene hybrid aerogels for supercapacitors with high energy density and long cycle life. J Mater Chem A, 2015, 3: 1828–1832
37 Wang X, Lv L, Cheng Z, *et al.* High-density monolith of n-doped holey graphene for ultrahigh volumetric capacity of Li-ion batteries. Adv Energy Mater, 2016, 6: 1502100
38 Feng J, Sun X, Wu C, *et al.* Metallic few-layered VS_2 ultrathin nanosheets: high two-dimensional conductivity for in-plane supercapacitors. J Am Chem Soc, 2011, 133: 17832–17838
39 Peng L, Peng X, Liu B, *et al.* Ultrathin two-dimensional MnO_2/graphene hybrid nanostructures for high-performance, flexible planar supercapacitors. Nano Lett, 2013, 13: 2151–2157
40 Gao S, Sun Y, Lei F, *et al.* Ultrahigh energy density realized by a single-layer β-$Co(OH)_2$ all-solid-state asymmetric supercapacitor. Angew Chem Int Ed, 2014, 53: 12789–12793
41 Zhu Y, Murali S, Cai W, *et al.* Graphene and graphene oxide: synthesis, properties, and applications. Adv Mater, 2010, 22: 3906–3924
42 Li L, Peng S, Wu HB, *et al.* A flexible quasi-solid-state asymmetric electrochemical capacitor based on hierarchical porous V_2O_5 nanosheets on carbon nanofibers. Adv Energy Mater, 2015, 5: 1500753–1500760
43 Kong D, Li X, Zhang Y, *et al.* Encapsulating V_2O_5 into carbon nanotubes enables the synthesis of flexible high-performance lithium ion batteries. Energy Environ Sci, 2016, 9: 906–911
44 Wu J, Gao X, Yu H, *et al.* A scalable free-standing V_2O_5/CNT film electrode for supercapacitors with a wide operation voltage (1.6 V) in an aqueous electrolyte. Adv Funct Mater, 2016, 26: 6114–6120
45 Kim D, Yun J, Lee G, *et al.* Fabrication of high performance flexible micro-supercapacitor arrays with hybrid electrodes of MWNT/V_2O_5 nanowires integrated with a SnO_2 nanowire UV sensor. Nanoscale, 2014, 6: 12034–12041
46 Wei Q, Liu J, Feng W, *et al.* Hydrated vanadium pentoxide with superior sodium storage capacity. J Mater Chem A, 2015, 3: 8070–8075
47 Moretti A, Passerini S. Bilayered nanostructured $V_2O_5{\cdot}nH_2O$ for metal batteries. Adv Energy Mater, 2016, 6: 1600868
48 Song Y, Zhao W, Kong L, *et al.* Synchronous immobilization and conversion of polysulfides on a VO_2–VN binary host targeting high sulfur load Li–S batteries. Energy Environ Sci, 2018, 11: 2620–2630
49 Chen K, Xue D. High energy density hybrid supercapacitor: *in-situ*

functionalization of vanadium-based colloidal cathode. ACS Appl Mater Interfaces, 2016, 8: 29522–29528
50 Watanabe T. Characterization of vanadium oxide sol as a starting material for high rate intercalation cathodes. Solid State Ion, 2002, 151: 313–320
51 Perera SD, Patel B, Nijem N, *et al.* Vanadium oxide nanowire-carbon nanotube binder-free flexible electrodes for supercapacitors. Adv Energy Mater, 2011, 1: 936–945
52 Bauhofer W, Kovacs JZ. A review and analysis of electrical percolation in carbon nanotube polymer composites. Compos Sci Tech, 2009, 69: 1486–1498
53 Lv G, Wu D, Fu R, *et al.* Electrochemical properties of conductive filler/carbon aerogel composites as electrodes of supercapacitors. J Non-Crystalline Solids, 2008, 354: 4567–4571
54 Wu NL, Wang SY. Conductivity percolation in carbon-carbon supercapacitor electrodes. J Power Sources, 2002, 110: 233–236
55 Yu P, Zhao X, Huang Z, *et al.* Free-standing three-dimensional graphene and polyaniline nanowire arrays hybrid foams for high-performance flexible and lightweight supercapacitors. J Mater Chem A, 2014, 2: 14413–14420
56 Yan J, Wang Q, Wei T, *et al.* Template-assisted low temperature synthesis of functionalized graphene for ultrahigh volumetric performance supercapacitors. ACS Nano, 2014, 8: 4720–4729
57 Lukatskaya MR, Mashtalir O, Ren CE, *et al.* Cation intercalation and high volumetric capacitance of two-dimensional titanium carbide. Science, 2013, 341: 1502–1505
58 Yan J, Wang Q, Lin C, *et al.* Interconnected frameworks with a sandwiched porous carbon layer/graphene hybrids for supercapacitors with high gravimetric and volumetric performances. Adv Energy Mater, 2014, 4: 1400500–1400509
59 Zhao MQ, Ren CE, Ling Z, *et al.* Flexible MXene/carbon nanotube composite paper with high volumetric capacitance. Adv Mater, 2015, 27: 339–345
60 Yu ZY, Chen LF, Song LT, *et al.* Free-standing boron and oxygen co-doped carbon nanofiber films for large volumetric capacitance and high rate capability supercapacitors. Nano Energy, 2015, 15: 235–243
61 Long C, Chen X, Jiang L, *et al.* Porous layer-stacking carbon derived from in-built template in biomass for high volumetric performance supercapacitors. Nano Energy, 2015, 12: 141–151
62 Jiang L, Sheng L, Long C, *et al.* Densely packed graphene nanomesh-carbon nanotube hybrid film for ultra-high volumetric performance supercapacitors. Nano Energy, 2015, 11: 471–480
63 Jung N, Kwon S, Lee D, *et al.* Synthesis of chemically bonded graphene/carbon nanotube composites and their application in large volumetric capacitance supercapacitors. Adv Mater, 2013, 25: 6854–6858

Acknowledgements This work was supported by the National Natural Science Foundation of China (51702048 and 21603157), the National Basic Research Program of China (2015CB932600), and Jiangxi Provincial Department of Education (GJJ170459 and GJJ170457).

Author contributions Guo K performed the experiments; Li Y and Li C conducted the characterization; Yu N and Li H performed the data analysis; all authors contributed to the discussion and preparation of the manuscript. The final version of the manuscript was approved by all authors.

Conflict of interest The authors declare no conflict of interest.

Supplementary information Supporting data are available in the online version of the paper.

Kai Guo received his PhD degree in material science from Huazhong University of Science and Technology in 2017 and then joined the School of Chemistry, Biology and Materials Science, East China University of Technology. His research interest focuses on material synthesis and device design of flexible supercapacitors and aqueous batteries.

Neng Yu received her PhD degree from Huazhong University of Science and Technology in 2015. Currently, she works in the School of Chemistry, Biology and Materials Science, East China University of Technology. Her research interest is in the field of electrochemical energy materials and devices, with a focus on hybrid nanomaterials, supercapacitors and lithium ion batteries.

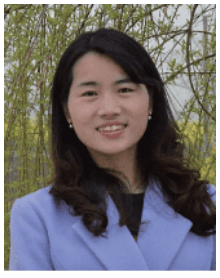

Huiqiao Li received her BSc degree in chemistry from Zhengzhou University in 2003, and then received her PhD degree in physical chemistry from Fudan University in 2008. Afterwards, she worked for 4 years at Energy Technology Research Institute, National Institute of Advanced Industrial Science and Technology (AIST), Japan. Currently, she is a full Professor of School of Materials Science and Engineering, Huazhong University of Science and Technology (HUST). Her research interest includes energy storage materials and electrochemical power sources such as lithium-ion batteries, sodium-ion batteries and supercapacitors.

高密度层状自支撑$V_2O_5{\cdot}nH_2O$/CNTs一维二维复合薄膜用于高体积容量柔性超级电容器

郭凯[1,4], 李一举[2], 李冲[3], 喻能[1*], 李会巧[4*]

摘要 柔性超级电容器是一种引人注目的可穿戴设备的储能器件，但是其较低的体积能量密度限制了其应用. 二维非碳基纳米材料是目前制备高体积容量超级电容器最有前景的电极材料. 然而二维赝电容纳米材料导电性差且容易自发紧密堆叠，难以表现出理想的电化学性能. 本论文通过简单规模化的方法制备了大尺寸的$V_2O_5{\cdot}nH_2O$超薄纳米片，并与一维碳纳米管复合制备成高密度的层状薄膜. 当碳纳米管的质量分数达到10%时，复合薄膜中发生电荷渗透效应导致电子导电性大幅提升，同时$V_2O_5{\cdot}nH_2O$超薄纳米片被碳纳米管高效率分散，且复合薄膜依然具有高密度，因此这种自支撑的薄膜表现出高达521.0 F cm^{-3}的体积比容量. 基于复合薄膜制备的全固态柔性超级电容器拥有高达17.4 W h L^{-1}的体积能量密度.

